LOSS-OF-FUNCTION FGFR2 MUTATIONS IN MELANOMA

Michael G. Gartside[1], Huaibin Chen[2], Omar A. Ibrahimi[2], Sara A. Byron[1], Amy V. Curtis[1], Candice L. Wellens[1], Ana Bengston[1], Laura M. Yudt[3], Anna V. Eliseenkova[2], Jinghong Ma[2], John A. Curtin[4], Pilar Hyder[1], Ursula L. Harper[3], Erica Riedesel[3], Graham J. Mann[5], Jeffrey M. Trent[6], Boris C. Bastian[4], Paul S. Meltzer[3], Moosa Mohammadi[2], Pamela M. Pollock[1]

[1] Cancer and Cell Biology Division, Translational Genomics Research Institute, Phoenix, AZ, 85004. USA

[2] Department of Pharmacology, New York University School of Medicine, 550 First Avenue, New York, NY 10016, USA.

[3]Genetics Branch, Center for Cancer Research, National Cancer Institute, National Institutes of Health, Bethesda, Maryland 20892, USA.

[4] Comprehensive Cancer Center, University of California, San Francisco, San Francisco, CA 94143-0808, USA.

[5] Westmead Institute for Cancer Research, University of Sydney, Westmead Millennium Institute, Westmead, NSW 2145, Australia.

[6] Genetic Basis of Human Disease Division, Translational Genomics Research Institute, Phoenix, AZ, 85004. USA

Address Correspondence to: P. Pollock PhD TGen 445 N 5th St, Phoenix AZ 85004 USA.
Email: ppollock@tgen.org

KEY WORDS: Melanoma, mutation, FGFR2, mislocalization, loss of function

Abstract

We report that 10% of melanoma tumors and cell lines harbor mutations in the FGFR2 gene. These novel mutations include three truncating mutations and 20 missense mutations occurring at evolutionary conserved residues in FGFR2, as well as among all four FGFRs. The mutation spectrum is characteristic of those induced by UV radiation. Mapping of these mutations onto the known crystal structures of FGFR2, followed by *in vitro* and *in vivo* studies show these mutations result in receptor loss of function through several distinct mechanisms, including loss of ligand binding affinity, impaired receptor dimerization, destabilization of the extracellular domains and reduced kinase activity. To our knowledge this is the first demonstration of loss-of-function mutations in a Class IV receptor tyrosine kinase (RTK) in cancer. Taken into account

with our recent discovery of activating FGFR2 mutations in endometrial cancer, we suggest that FGFR2 may join the list of genes that play context-dependent opposing roles in cancer.

Introduction

Melanoma is the most lethal of all skin cancers. The American Cancer Society estimated that there would be 59,940 new cases of melanoma and about 8,110 deaths due to melanoma in 2007. Previous studies in human melanocytes and melanoma cells have revealed that one of the hallmarks of melanocytic transformation is a change from paracrine growth factor stimulation by the surrounding keratinocytes in the skin to autocrine growth factor stimulation via ectopic expression of growth factors and/or receptors by melanoma cells (1, 2). FGF signaling plays a prominent role in tissue homeostasis by providing bidirectional paracrine communication between mesenchymal and epithelial cells of parenchymal organs including skin. The FGF family comprises 18 ligands (FGF1-FGF10 and FGF16-FGF23) which signal through four transmembrane receptor tyrosine kinases (FGFR1-FGFR4) and their tissue specific alternatively spliced b (epithelial) and c (mesenchymal) isoforms (3). Previous studies have demonstrated that survival and proliferation of melanocytes depends on FGF2 which is provided by the surrounding keratinocytes in the skin. A number of functional studies have implicated both FGF2 and FGFR1 signaling in melanoma progression. Adenoviral transduction of melanocytes with FGF2 resulted in phenotypic changes consistent with increased tumorigenicity (4, 5) and downregulation of FGF2 via antisense oligonucleotides in metastatic melanoma inhibited proliferation and colony formation in soft agar (6, 7). Introduction of antisense oligonucleotides targeted towards FGFR1 into melanocytes and metastatic melanoma cell lines resulted in decreased proliferation and signs of differentiation (8, 9). Furthermore, injection of an antisense FGFR1 construct into primary and metastatic melanomas grown in nude mice has also been shown to result in inhibition of tumor growth and induction of apoptosis (10, 11).

Constitutive activation of FGFRs through chromosomal translocation, aberrant splicing,

or missense mutations has been reported in several cancers. The Catalog of Somatic Mutations in Cancer (COSMIC) provides a repository of all somatic changes reported to date in this receptor family (http://www.sanger.ac.uk/genetics/CGP/cosmic/). To date FGFR3 is mutated at highest frequency in benign seborrheic keratoses and bladder cancer and to a lesser extent in multiple myeloma, and cervical cancer. We have recently reported the presence of activating mutations in FGFR2 in 16% of endometrioid endometrial cancers (12).

We report here the identification of novel FGFR2 mutations in 15/113 (13%) of melanoma cell lines and 8/100 (8%) of uncultured melanoma tumors. Mapping of these mutations onto the known crystal structures of FGFR2 together with *in vitro* and *in vivo* functional analyses show that these mutations result in receptor loss of function.

Results

Identification of FGFR2 mutations in melanoma cell lines and uncultured primary and metastatic melanoma tumors

We screened an initial panel of 47 melanoma cell lines for the presence of mutations in the FGFR1-4 genes by sequencing. Following the identification of mutations in FGFR2, 66 additional melanoma cell lines were screened for FGFR2 mutations using a combination of dHPLC and sequencing leading to the identification of fifteen different FGFR2 mutations (Table 1). None of these mutations were observed in a panel of lymphocyte DNA from 150 Caucasian controls (data not shown), suggesting that these mutations arose somatically. Of the 15 cell lines carrying FGFR2 mutations, 11 also carried mutations in either BRAF or NRAS (Table 1). No mutations were identified in either FGFR1 or FGFR3, while one mutation at a non-conserved codon was found in FGFR4, P716R.

Next, we screened a panel of 28 metastatic melanoma tumors and a panel of 72 vertical growth phase (VGP) primary melanomas representing samples from different melanoma subtypes for the presence of mutations in FGFR2 gene. We identified mutations in 3/28

metastatic samples and 5/72 primary tumors respectively (Table 1). Subset analysis revealed FGFR2 mutations in 1/17 (6%) superficial spreading melanomas (SSM), 2/10 (20%) lentigo maligna melanomas (LMM), 1/28 (4%) acral melanomas (AM), and 1/17 (6%) mucosal melanomas (MM). For three of these tumors, we were able to extract DNA from surrounding normal tissue and in all cases the mutation was only present in the tumor, confirming the somatic origin of these mutations. Reminiscent of the "mutator phenotype" seen in the breast cancer kinome screen (13), one metastatic tumor was found to carry four different FGFR2 mutations (V77M, E574K, S688F, P708S), which were not further analyzed as there was a high probability that these mutations represented 'passenger' mutations rather than 'driver' mutations. Notably, two primary tumors carried nonsense mutations (Table 1). The majority (20/22) of FGFR2 mutations occurred at residues that are conserved across FGFR1-4 or at residues that are conserved in 3/4 of the FGF receptors as well as conserved in FGFR2 across evolution (data not shown). Mutations in both NRAS and BRAF were observed in tumors with FGFR2 mutations at similar frequencies to that reported in the literature.

Mapping of FGFR2 mutations within known FGFR2 structures

Extracellular mutations

To gain insights into how the different FGFR2 mutations might impact receptor function, we analyzed them in the light of our crystallographic data on FGFRs. The E219K, G227E, V248D, R251Q and G271E mutations, which affect residues in the extracellular region of FGFR2, were mapped onto the crystal structure of the 2:2:2 FGF2-FGFR1c-heparin dimer (PDB entry 1FQ9) (14) (Figure 1). We intentionally chose this structure instead of the crystal structure of the 1:1 FGF2-FGFR2c monomer in order to evaluate the impact of the mutations on heparin/heparan sulphate (HS) and FGF-induced FGFR dimerization. In the dimer, two centrally located FGFRs interact with each other directly and each receptor makes contacts with both ligands as well.

Ligand interacts with the second and third immunoglobulin domains (hereafter referred to as D2 and D3) and the interconnecting D2-D3 linker. The R251Q mutation maps to the highly conserved D2-D3 linker region (Figure 1, panel B). In the structure, R250, the residue homologous to R251 of FGFR2, makes three hydrogen bonds with its primary FGF2 suggesting that the R251Q mutation should diminish the binding affinity of FGFR2 towards FGF2 (Figure 1, panel B). By contrast, the E219K mutation maps to the secondary ligand binding site on D2. In the dimer, D218, which corresponds to E219 of FGFR2, makes a hydrogen bond with K35 of the secondary FGF2 ligand (Figure1, panel E). Therefore, based on the structure, E219K should not affect the ability of FGFR2c to bind FGF2, but it should reduce the ability of FGFR2 to undergo FGF and heparin-induced dimerization.

Other extracellular mutations including V248D, G227E and G271E are predicted to destabilize the tertiary fold of either D2 (V248D and G227E) or D3 (G271E). V247, which corresponds to V248 of FGFR2, is situated at the C-terminal end of the βG strand in D2 where its side chain is surrounded by other hydrophobic residues inside the hydrophobic core of D2 (Figure 1, panel A). Substitution of V248 with the charged aspartic acid should be detrimental to the tertiary folding of D2. G226, which corresponds to G227 in FGFR2c, maps to the start of the βF strand in D2 and spatially is in close vicinity to V247 (Figure 1, panel A). G270, which corresponds to G271 in FGFR2, maps to the loop between the βA' and βB strands in D3 (Figure 1, panel C). Each glycine residue provides hydrogen bonds that contribute to the proper β strand formation in D2 and D3, respectively. Therefore, based on the structure, these substitutions should cause local structural perturbations, which could ultimately impact the folding of the whole D2 and D3 respectively. Destabilization of D2 and D3 is predicted to impair the correct intramolecular disulphide bridge formation in D2 or D3, leading to exposure of the conserved cysteines and allowing them to form intermolecular disulfide-bridged receptor dimers.

This destabilization can also interfere with the correct processing/maturation and trafficking of the mutated receptor through the ER/Golgi, resulting in receptor mislocalization.

Based on the structure, the E160A and H213Y mutations are likely to impact the interaction of FGFR2 with HS. In the structure, E159 of FGFR1, which corresponds to E160 of FGFR2, facilitates the conformation of gA helix in D2, on which a key lysine residue involved in HS binding resides (Figure 1, panel D). Therefore, destabilization of the gA helix due to the E160A mutation should negatively impact FGFR2-HS interaction and thereby attenuate FGF- and HS-mediated FGFR dimerization. T212, the residue corresponding to H213 of FGFR2, points into the heparin binding canyon of the 2:2:2 FGF2-FGFR1-HS dimer (Figure 1, panel D) and the bulkier tyrosine side chain at this location could cause steric clashes with HS oligosaccharide molecules leading to inefficient receptor dimerization.

Kinase domain mutations

Over half of the melanoma mutations affect the conserved tyrosine kinase domain of FGFR2, and mapping of these mutations onto unphosphorylated and phosphorylated FGFR2 kinase domain structures (PDB ID: 2PSQ and 2PVF)(15) suggests that they also represent loss-of-function mutations (Figure 2). Notably, M640 and I642 localize onto either end of the βb8 strand (Figure 2, panel B), a secondary structure element that precedes the activation loop (A-loop) of the kinase domain. The hydrophobic side chains of these residues are in contact with residues in the αE helix in the inner most core of the C-lobe of the kinase domain. Substitutions of either residues with the smaller hydrophobic residues isoleucine or valine respectively would cause a cavity within the core of the kinase that should induce local structural perturbations that ultimately impact the conformation of the activation loop. The A648T mutation maps to the activation loop of the kinase domain (Figure 2, panel E) and is also expected to lead to loss of function. This is because in the phosphorylated activated kinase domain of FGFR2 (PDB ID:

2PVF)(15), the methyl group of A648 makes hydrophobic contact with M537 in the αC helix which contributes to the correct positioning/orientation of the αC helix relative to the C-terminal lobe of the kinase, and hence to the productive alignment of the catalytic residues for the phosphotransfer reaction (15). A threonine is unfavorable at this location as its larger side chain is predicted to sterically hinder the αC helix from approaching sufficiently close to the C-terminal lobe and consequently, the catalytic residues would not be aligned for the phosphotransfer reaction.

The E636K mutation maps to the loop region between the β7 and β8 strands (Figure 2, panel A). In the structure, the side chain of E636 makes a solvent-exposed hydrogen bond with S568 which is located in the hinge region of the kinase domain, suggesting that it may play a role in regulation of the spatial positioning of the N-terminal and C-terminal lobes of the kinase relative to each other. Based on the structure, the E636K mutation should influence the kinase activity of the FGFR2 kinase domain. The E475 is part of the WE consensus motif that defines approximately the N-terminal boundary of the conserved kinase domain in many receptor tyrosine kinases. E475 engages in two strong hydrogen bonds with T555, whose methyl group is in hydrophobic contact with residues in αC helix (Figure 2, panel D). Hence, these interactions hold the αC helix in an orientation found in unphosphorylated inhibited kinases. In the phosphorylated activated kinase domains, however, these hydrogen bonds are weaker and concomitantly the C-helix moves closer towards C-lobe. Loss of these hydrogen bonds due to the E475K mutation could relieve this inhibition and potentially lead to activation of the kinase domain. Alternatively, the E475K mutation could introduce structural instability in the N-lobe of the kinase and reduce the half life of the mutant FGFR2. The G701S mutation maps to the loop between αF and αG helices (Figure 2, panel F) and facilitates the conformation of this loop region, which makes several hydrogen bonds with K668 in the activation loop. Therefore, the structural perturbations induced by G701S mutation could indirectly lead to reduced kinase

activity. The R759Q mutation maps to the C-terminal end of αI helix, the last secondary structure element of the kinase domain. In the structure R759 makes hydrogen bonds with two other residues in its vicinity (Figure 2, panel C), and loss of these hydrogen bonds due to the R759Q mutation could also induce subtle structural changes leading to a loss in kinase activity.

The L770V mutation should reduce the ability of FGFR2 to activate PLCγ signaling pathway. L770 follows the Y769, the major phosphorylation site of FGFR2 which serves as the docking site for SH2 domains of PLCγ and thus is required for PLCγ phosphorylation and activation by the activated FGFR2. NMR solution structure of PLCγ SH2 domain in complex with phosphopeptide indicates that SH2 domain of PLCγ interacts with pTyr and residues +1 to +6 positions relative to the pTyr Hence, the L770V mutation should reduce the affinity of SH2 domains to the activated FGFR2. The L770V mutation could also reduce Y769 phosphorylation because the substrate binding pocket of the kinase domain prefers a leucine over a valine next to the tyrosine phosphorylation site (Chen and Mohammadi, unpublished results). The reduced phosphorylation of Y769 could in turn reduce the ability of FGFR2 to activate the PLCγ pathway. Table 2 summarizes the different mechanisms of loss of function by the melanoma mutations inferred from crystal structures. Consistent with these analyses predicting that the FGFR2 mutations are loss-of-function mutations, two melanoma samples harbored nonsense mutations and a third sample carried a splicing mutation that would result in premature termination of FGFR2 protein translation (Table1).

Analysis of FGFR2 melanoma mutations in vitro

To test our structural predictions for the extracellular mutations on FGFR2 function, we expressed recombinant wild type and mutant ectodomains in E. coli, isolated the inclusion bodies enriched in the proteins and subjected them to *in vitro* refolding. As a positive control we also used the S252W mutant ectodomain. We have previously shown that the S252W mutation

has no adverse effect on folding of FGFR ectodomain (16). We were unable to refold *in vitro* the ectodomain proteins containing the G227E, V248D, and G271E mutations consistent with structural predictions that these mutations are detrimental to the tertiary fold of D2 and D3 domains. By contrast, the R251Q mutant ectodomain folded *in vitro* with yields similar to those of the wild type and S252W mutant receptor. We then used surface plasmon resonance to analyze the effect of the R251Q mutation on ligand binding affinity of FGFR2c. Consistent with structural predictions, the R251Q mutation severely impaired the ability of FGFR2c to bind multiple FGF ligands including FGF2 (Figure 3) and FGF1, 4, 7, 8 and 10 (data not shown). On the other hand, as expected, the S252W mutation enhanced the affinity of FGFR2c towards FGF2 and other FGFs (16-18) (data not shown).

To test the impact of kinase domain mutations, we prepared recombinant wild type and mutant kinase domain proteins harboring the E475K, D530N, I642V, and A648T melanoma mutations and subjected them to *in vitro* kinase assays. Consistent with structural predictions, the D530N, I642V and A648T mutant kinase domains exhibited reduced kinase activity relative to the wild type kinase domain (Figure 4). Interestingly, the E475K mutant exhibited a slight increase in kinase activity relative to the wild-type kinase domain. Notably, the protein expression yield for the E475K mutant kinase was several fold less than that of wild type kinase, suggesting this mutation was partially destabilizing the kinase domain.

Analysis of FGFR2 mutations in cultured cells

We next analyzed the impact of several mutations (G227E, R251Q, G271E, E475K, D530N, I642V and A648T) on the receptor trafficking and maturation of the full length FGFR2c. Three different FGFR2 mutants harboring C278F, S252W or K517R served as controls. The C278F activating mutation associated with Crouzon Syndrome was used to assess the impact of destabilizing D3 on both receptor maturation and activation. This mutation has been shown to result in impaired receptor processing, constitutive dimerization and increased signaling from

intracellular compartments (19). In contrast, the S252W mutation observed in patients with Apert syndrome has no impact on receptor folding (18). The K517R mutant receptor served as a kinase deficient receptor. K517 coordinates the phosphate groups of ATP and its mutation to arginine in the homologous FGFR3 has been previously shown to abolish kinase activity (20).

Following transfection of wildtype FGFR2 receptor into HEK293 cells, two major FGFR2-immunoreactive bands (110kDa and 130kDa) are observed. PNGase digestion resulted in the reduction in size of both bands to a single 98KDa band (open arrow) confirming these two bands are differently glycosylated receptor populations (Figure 5a). $EndoH_f$ digestion, which is known to remove N-linked high mannose moieties but not complex carbohydrates from glycosylated proteins, resulted in the reduction of the 110kDa band to 98kDa but had no effect on the mobility of 130kDa band. These data show that the 110kDa form represents immature partially processed receptor present in the ER and early Golgi, whereas the $EndoH_f$ resistant 130kDa band represents the fully glycosylated mature receptor. Densitometric analysis indicates that the $EndoH_f$ resistant 130kDa mature form comprises ~60% of the wildtype FGFR2 (Figure 5a, 5b). The R251Q and S252W mutations did not reduce the relative proportion of EndoH resistant 130kDa mature form, which is fully consistent with our structural predictions of no adverse effects on protein stability by these mutations. In contrast, only 30% of G227E, V248D, G271E and C278F mutants were $EndoH_f$ resistant, suggesting impaired receptor processing of these FGFR2 mutants. This is also consistent with our structural predictions that these mutations will adversely impact structural integrity of D2 or D3 domain of FGFR2 (Figure 5b upper panel). There was a small increase in the relative proportion of the 110kDa band for the E475K mutant (Figure 5b, lower panel), consistent with the decreased protein yield observed in the in-vitro kinase assays.

To confirm altered cellular localization of the mutants, we performed immunofluorescence (IF) studies in transiently transfected HEK293 cells. In cells transfected with wildtype FGFR2, positive immunofluorescence signal was distributed primarily in the

plasma membrane and also in the rough ER and Golgi (Figure 5c). In cells transfected with the G227E mutant (Figure 5c) however, there was positive perinuclear staining, particularly evident around the nuclear membrane as well as a dispersed reticular staining indicative of retention in the ER. IF also demonstrated mislocalization to intracellular membrane and decreased cell surface expression for FGFR2 mutants V248D, G271E and C278F. In contrast, IF of the A648T mutant shows clear cell surface localization in keeping with the structural predictions and $EndoH_f$ analyses. To confirm the ER localization of the G227E mutant, we then performed similar IF studies looking for colocalization with the ER resident protein, protein disulphide isomerase (PDI) which revealed a high degree of colocalization of the two proteins confirming impaired receptor localization (Figure 5d). In contrast, marked cell surface localization and limited colocalization with PDI was observed for both the wildtype FGFR2 and the E219K mutation, predicted to have no detrimental effect on receptor folding.

BaF3 proliferation assay and p44/42 MAPK phosphorylation in response to FGF2 as readout of receptor function

We next analyzed the effects of the melanoma mutations on FGFR2c activity. Given that melanocytes and melanoma cell lines express other FGFRs whose activation may mask the ability to specifically evaluate FGFR2 signaling and function, we used the murine interleukin-3 dependent pro-B BaF3 cell line to determine receptor activity. The BaF3 cell line is routinely used as a model system for the evaluation of FGFR function, as it does not express endogenous FGF ligands or receptors. Although BaF3 cell proliferation and survival is normally dependent on IL-3, activated tyrosine kinase signaling can substitute for IL-3 to maintain cell viability and proliferation. We included the N549K FGFR2 receptor as a constitutively activated positive control as this activating mutation has been reported in endometrial cancer (12) and an identical mutation at the paralogous positions in FGFR3 has been associated with hypochondroplasia (N540K) (21). Polyclonal stable lines were generated following lentiviral

transduction and selection in Geneticin. Proliferation assays were then performed in the absence of IL3 and the presence of 1nM FGF-2 and 10ug/mL heparin and cell viability assayed after five days. As anticipated, the constitutively active N549K mutant resulted in levels of proliferation above that achieved by the wildtype receptor, whereas expression of all mutant constructs including G227E, G271E, E475K, I642V and A648T FGFR2 resulted in reduced cell proliferation compared to wildtype FGFR2 (Figure 6a), verifying that these mutations impaired or abrogated the ability of FGFR2 to stimulate cell proliferation in response to ligand in an *in vivo* setting. Surprisingly, the N549K mutation did not cause constitutive BaF3 proliferation in the absence of ligand stimulation.

As a further assessment of receptor impairment due to mutation, we examined the ability of the receptor to activate the pro-proliferative p44/42 MAPK signaling pathway in response to exogenous rFGF2. With the exception of the N549K known activating mutant, all mutations resulted in a reduction to varying levels in the ability of the receptor to induce phosphorylation of p44/42 MAPK. (Figure 6 b, c & d)

Reintroduction of FGFR2 into melanoma cells

We next sought to determine whether reintroduction of FGFR2 could suppress proliferation of melanoma cells. RTPCR with isoform specific primers and subsequent sequencing revealed normal human melanocytes and the majority of melanoma cell lines expressed the mesenchymal FGFR2c isoform (data not shown). For this reason our reintroduction studies utilized the FGFR2c isoform. We overexpressed FGFR2c in melanoma cell lines that lacked FGFR2 expression by RT-PCR (SbCl2), and in melanoma cell lines that expressed mutant FGFR2 (AO4, D22, UACC2534) and assessed proliferation. Surprisingly, reintroduction of FGFR2 failed to suppress proliferation of these melanoma cell lines (Figure 7a). Expression of FGFR2 following lentiviral transduction was confirmed by Western blot analysis for each cell line

(Figure 7b). Similar results were also achieved in both the D22 and UACC2534 melanoma cell lines (data not shown).

Discussion

In this study we report novel FGFR2 mutations in 15/116 melanoma cell lines and 8/100 uncultured metastases and primary tumors. In order to determine the ratio of non-synonymous to synonymous mutations in our dataset, we went back and examined the synonymous variants we identified. As we did not have constitutional DNA for these samples, we excluded them as probable somatic mutations if they had been previously identified in dbSNP. Several additional synonymous variants occurred alongside each other in multiple individuals, consistent with the presence of a rare germline haplotype block. Following the exclusion of these putative SNPs, 4 synonymous variants remained, therefore the conservative ratio of non-synonymous to synonymous mutations in our dataset was 23:4, which exceeds the 2:1 ratio one would expect if these were random passenger mutations and supporting a role for these mutations in melanoma pathogenesis. Furthermore, the mutations spectrum is characteristic of those induced by UV radiation, namely 70% of the mutations were C:G>T:A substitutions with one CC:GG>TT:AA tandem mutation. The presence of characteristic UV mutations in FGFR2 suggest that mutation of this gene is possibly an early event in transformation, and we anticipate that further sequencing analysis in a greater number of primary tumors and nevi will shed light on when during melanoma development these mutations arise. It should be noted that the mutation frequency reported in this study may be an underestimate. This is based on the fact that 40 cell lines were screened by dHPLC rather than sequencing, exons 2-5 were not screened in this latter panel of cell lines, and not all primary tumors provided high quality sequence for all exons.

Insights gained from mapping these mutations onto known FGFR2 crystal structure, combined with *in vitro* and *in vivo* functional studies show that these mutations lead to loss of

receptor activity through different mechanisms, including loss of ligand binding (R251Q); incomplete processing of the receptor and retention in the ER (V248D, G227E, G271E); and complete or partial loss of tyrosine kinase activity (A648T, D530N, I642V). Future studies confirming the structural predictions described herein may also reveal that FGFR2 loss-of-function can occur through impaired FGF and HS induced receptor dimerization and reduced binding to PLCγ.

The loss of function nature of our identified melanoma mutations is also consistent with published literature. In support of D530N resulting in FGFR2 loss-of-function, a germline D771N mutation at the equivalent codon in RET has been associated with Hirschsprung's disease, commonly due to loss-of-function mutations in RET (22). Also, while these studies were underway, the A648T FGFR2 mutation was identified in the germline of affected patients in two independent families with autosomal dominant lacrimo-ariculo-dento-digital (LADD) syndrome (OMIM 149730) (23). Consistent with our in vitro and in vivo data a recent study showed that the A648T mutation abrogated tyrosine kinase activity of FGFR2 (24). As discussed earlier, we propose that this mutation creates a steric barrier for the movement of the kinase N-lobe towards the C-lobe which is predicted to take place when the kinase transits from the basal "low" activity state to the "active" state. However, precise definition of the mechanism by which A648T mutation impairs FGFR2 kinase activity awaits the resolution of crystal structure of the mutant kinase domain as was recently carried out for an A628T LADD mutation. In contrast to the A648T mutation, the A628T mutation maps onto the catalytic loop of the kinase domain and the crystal structure of the mutant kinase shows that this mutation acts by introducing steric conflicts that alter the productive arrangement of the neighboring key catalytic residues (25).

A comparison of the mutations identified in melanoma to those our lab previously identified in endometrial cancer highlights the differences in the mutation spectra (Figure 8). The majority of the endometrial mutations (17/20) are identical to FGFR2 and FGFR3 mutations

previously reported in the germline, a finding similar to that observed for FGFR3 where a comparison of FGFR3 mutations reported in cancer with germline mutations associated with skeletal disorders shows a remarkable concordance, reviewed in (26, 27). In contrast, the more than 20 FGFR2 mutations we identified in melanoma were all novel, supporting our findings that the mutations are distinct and different from the many gain-of-function mutations previously identified in the FGFRs.

This discovery of loss of function mutations in an RTK is unexpected, given the conventional wisdom that activation of receptor tyrosine kinases (eg KIT, FLT3 and FGFR3) drive tumorigenesis and our previous report documenting the presence of activating mutations in FGFR2 in endometrial cancer (12). However, it should not be surprising given that a variety of RTK signaling pathways can induce either proliferation or differentiation depending on the cell type. Indeed, Cre-Lox transgenic mice where FGFR2b has been deleted in cells expressing keratin V develop spontaneous papillomas. Moreover, following DMBA and TPA treatment, these transgenic mice developed an increased number of papillomas and carcinomas compared to widltype mice, providing support that FGFR2 can act as a tumor suppressor gene in some cell types (28). Furthermore, loss of FGFR2 expression has been associated with several cancers including prostate and bladder (29-31). Reintroduction of FGFR2 resulted in decreased growth in vitro and reduced tumorigenicity in vivo of bladder carcinoma cells (32), prostate tumor cells (33-35) and salivary adenocarcinoma cells (36).

Based on these data and our structural, biochemical and biological data supporting the characterization of the FGFR2 mutations identified in melanoma as loss of function, it was indeed surprising that reintroduction of FGFR2 failed to suppress proliferation of melanoma cell lines. There are several possible explanations for these apparent disparate results. One difference between the previously published reintroduction results and the current melanoma study is that they involve different FGFR2 spliceforms. The previous studies were all carried out in cells of epithelial origin with the FGFR2 IIIb isoform whereas our studies evaluated

proliferation following reintroduction of FGFR2 IIIc, the isoform of FGFR2 expressed in mesenchymal cells and in the melanocytes, which are derived from the neural crest. The lack of suppression of proliferation of melanoma cells following overexpression of FGFR2 may therefore reflect a cell lineage specific function of FGFR2. Another possible explanation is that loss or abrogation of FGFR2 is an early event and those melanoma cell lines have acquired additional genetic aberrations that prevent suppression of proliferation following FGFR2 reintroduction. Alternatively, abrogation of FGFR2 may not contribute to melanoma pathogenesis by removing a growth inhibitory signal. Indeed, though tumor suppressors classically function to regulate cell cycle, accumulating evidence suggests that additional subsets of genes exist which function to suppress tumorigenesis not by inhibiting proliferation, but by altering other aspects of the malignant phenotype, including loss of contact inhibition, angiogenesis, cell migration, and metastasis. Therefore, the pathogenic consequence of loss of FGFR2 function may not directly involve cell cycle regulation, but instead impact another aspect of tumorigenesis. The caveat exists that loss of FGFR2 might not be a driver of cell transformation but rather these mutations occur as a consequence of the oncogenic state, however their selection in 10% of melanoma samples would argue that they must provide a selective advantage to the cells in which they arose. This is consistent with a relatively high frequency and high non-synonymous to synonymous ratio arguing against their presence as passenger mutations.

Elucidation of the mechanism by which FGFR2 contributes to melanoma is also complicated by our current lack of understanding as to the differing cellular functions of the multiple splice forms of these receptors, particularly in the melanocytic system. There are additional splice variants affecting the ligand binding domain (2 Ig, 3 Ig), cytoplasmic juxtamembrane domain (+VT, -VT), and C-terminal domain of FGFR2 (C1, C3), and the role of these splice variants in normal melanocyte function and melanoma pathogenesis is currently unknown. Our lab is currently investigating the relative expression levels of these various

isoforms and their functional significance in melanocytes and melanoma. FGFR2 may also have cellular functions distinct from typical RTK signaling. There have been reports that FGFR1 binds CBP and RSK in the nucleus (37) and we and others have observed FGFR2 localized to the nucleus in various cell types (unpublished results) (38). Lastly we and others have shown that FGFR2 can heterodimerize with FGFR1 at least in vitro (unpublished results) (39) and FGFRs have also been shown to bind to other molecules at the cell surface including NCAM (40). We postulate that a more complete understanding of FGFR biology will allow us to identify the mechanism by which loss of FGFR2 contributes to melanoma initiation and/or progression.

In conclusion, we provide strong genetic, biochemical, in vitro and in vivo evidence that loss of function FGFR2 mutations occur in a subset of melanomas. Though we have yet to uncover the biological consequence of loss of FGFR2 function in melanoma, we propose that FGFR2 should join the list of those genes that play context dependent opposing roles in tumorigenesis. Although many genes have been shown to have context dependent opposing roles in cancer eg Notch, TGFβ (41), FGFR2 may be the first gene in which both loss and gain of function mutations have been reported in different tissue types. Ongoing work in our laboratory is targeted towards understanding the molecular mechanisms by which loss of FGFR2 contributes to melanoma pathogenesis.

Experimental Procedures

See Supplemental Methods for details regarding mutation detection.

Expression, refolding and purification of ectodomain of FGFR2

DNA fragment encoding residues 147 to 366 of FGFR2c was amplified by PCR and subcloned into pET-28a bacterial expression vector using NcoI and HindIII cloning sites. Point mutations (G227E, V248D, R251Q, S252W and G271E) were introduced using QuikChange site-directed mutagenesis kit (Stratagene). BL21(DE3) competent cells were transformed with wild type or

mutant expression constructs and protein expression was induced with 1mM IPTG for 5 hours at 37°C. Cells were lysed using French press, centrifuged, and the inclusion bodies containing wild type or mutant proteins were dissolved in 6 M guanidinium hydrochloride plus 10 mM DTT in 100 mM Tris-HCl buffer (pH 8.0). The solubilized FGFR2 proteins were subjected to an in vitro refolding by slow dialysis against 25 mM HEPES buffer (pH 7.5) containing 150 mM NaCl, 10% Glycerol, and L-Cysteine. The correctly refolded wild type and mutant proteins were then sequentially purified by heparin affinity and size exclusion chromatography. SPR analysis was performed as described previously (18).

Expression and purification of FGFR2 kinase domain

The DNA fragment encoding residues 458 to 768 of human FGFR2 was subcloned into pET bacterial expression vectors with an N-terminal 6XHis-tag to aid in protein purification. Point mutations (E475K, D530N, I642V, and A648T) were introduced using QuikChange site-directed mutagenesis kit (Stratagene). The bacterial strain BL21(DE3) cells were transformed with wild type or mutant FGFR2 kinase expression constructs and protein expression was induced with 1 mM IPTG for 4 hours at ambient temperature. The cells were then lysed using a French press, and the soluble kinase proteins were purified by using sequential Ni^{2+}-chelating, anion exchange and size exclusion chromatography. The purity of the proteins was estimated to be over 98% based on SDS-PAGE analysis. Purified wild type and mutant kinase proteins were concentrated to at least 10 mg/ml using a Centricon-10. The autophosphorylation activity of the wild type and mutant kinases was compared using a continuous spectrophotometric kinase assay according to the published protocol (42).

Site-directed mutagenesis of full length FGFR2

All mutations were introduced to the pcDNA3_FGFR2 wildtype plasmid (NM_000141) using the Quikchange II XL Site Directed Mutagenesis Kit (Stratagene) according to manufacturers

instructions. Additionally, mutagenesis primers were designed to introduce a novel, but silent (non-coding change) restriction enzyme (RE) recognition site to allow for fast, preliminary screening of clones. The full list of primer sequences can be found in Supplementary Table 1 online. After RE screening, the entire coding sequence of FGFR2 was sequenced for each clone to confirm the presence of the intended mutation and to ensure that no other mutations were introduced during the mutagenesis process. Plasmid DNA was then isolated using Qiagen EndoFree Plasmid DNA Isolation kits and DNA with A260/280 >1.8 was used in all subsequent experiments.

Cell lines and transfections

All cell lines described in this series of experiments were maintained under standard culturing conditions as described by the ATCC or DSMZ (Germany; BaF3 cell line). Transient transfections of 1ug total DNA (constisting of 250 ug wildtype or mutant FGFR2 + 750 ug empty plasmid) were achieved with FuGene 6 (Roche) at a 3:1 ratio of reagent:DNA according to manufacturers instructions.

Cell Lysis, Endoglycosidase digestions and Western blotting

Thirty six to 48 hours post transfection, cells were washed with ice-cold PBS and lysed in ice-cold lysis buffer (20 mM Hepes pH 7.4, 1% Triton X100, 2 mM EGTA, 10% glycerol, Complete Protease Inhibitor Cocktail (Roche), 1 mM NaF, 1 mM Na_3VO_4, 100 uM PMSF). For PNGase and $EndoH_f$ digestions, 20 ug of lysate was subjected to digestion according to manufacturers recommendations. Protein was resolved on 3-8% Tris acetate gels and transferred to PVDF membranes (Invitrogen). After blocking the membranes with 5% skim milk/TBST, membranes were probed with 1:2000 Bek C-17 (Santa Cruz Biotechnology).

Immunofluorescence

Cells were transfected as described and plated onto 8-well chamber slides. After 36-48 hours they were fixed with 4% paraformaldehyde, permeabilized in 0.2% Triton and incubated with 1:300 Bek C-17 and 1:1000 anti-PDI (Invitrogen) and detected with goat ant-rabbit Cy3 (1:200; Jackson ImmunoResearch) and goat anti-mouse AlexaFluor 488 (1:1000; Invitrogen) respectively. Slides were mounted with Pro Long Gold antifade reagent and imaged on a Zeiss LSM 5 Pascal confocal microscope.

Lentivirus production

293FT cells on poly-D-lysine coated plates were transfected with lentiviral packaging vectors and pTYF.FGFR2.IRES.Neo (or mutant FGFR2) using Superfect (Qiagen) at a 4:1 Superfect:DNA ratio as per manufacturers instructions. Media containing the virus was collected at 24 and 40 hours, pooled, filtered through a 0.45 um low protein binding filter and stored at -80^{o}C until use. Viral stocks were tittered in HEK293 cells following serial dilution in a six well plate, selection for fourteen days in 800ug/ml Geneticin, staining with crystal violet and colony counting.

BaF3 Proliferation assays

5 x 10^5 BaF3 cells were infected with an MOI of 1 (5 x 10^5 viral transducing units (TU)) for 23 hours, then placed under selective pressure (1200 ug/mL Geneticin) for 14 days in the presence of 5 ng/ml IL3. Transduced stably selected BaF3 cells containing wildtype and mutant FGFR2 were maintained under selection in RPMI/10% FBS containing 50 nM beta-mercaptoethanol,100U/mLpenicillin/100ug/mL streptomycin sulfate, 1000 ug/mL Geneticin and supplemented with 5 ng/mL murine IL-3 (R & D Sytems). Prior to the proliferation assay, cells were counted and washed in the above media containing no IL-3. Cells were plated at 1 x 10^4/well in triplicate in a 96 well plate, in media containing 16.7 ng/mL (1 nM) FGF-2 and 10 ug/mL heparin. Half the volume of media was removed at day 3 and replaced with an equal

volume containing fresh ligand at 2X concentration and no IL-3. Proliferation was assessed using the ViaLight Plus Cell Proliferation/Cytotoxity Kit (Lonza Rockland, Inc.) according to the manufacturer's instructions.

Melanoma proliferation assays

SbCl2 melanoma cells were cultured in 2% Tumor Medium containing a 4:1 mixture of MCDB 153 medium with 1.5 g/L sodium bicarbonate and Leibovitz's L-15 medium with 2 mM L-glutamine supplemented with 0.005 mg/ml bovine insulin, 1.68 mM CaCl2, and 2% fetal bovine serum. AO4, D22, and UACC2534 cells were grown in RPMI supplemented with 10% FBS. SbCl2, AO4, D22, and UACC2534 melanoma cells were transduced with empty vector, FGFR2, or kinase dead FGFR2 (K517R) at an MOI of 2 in the presence of 6 ug/ml polybrene. Cells were selected for at least 14 days in 500-800 ug/ml G418. 2,000-4,000 cells were plated per well in a 96 well plate in full growth media. The next day, cells were washed in PBS and switched to low serum media overnight (0.5% FBS for SbCl2 and 1% for AO4, D22, and UACC2534). Cells were then stimulated with 10ng/ml FGF2 and 10 ug/ml heparin in low serum media and proliferation assessed using the sulforhodamine B (SRB) assay. Fresh FGF2 and heparin were added on day 4.

p44/42 Phosphorylation

To examine p44/42 MAPK phosphorylation, cells were washed in PBS and resuspended in BaF media containing no FBS and no IL-3 (BaF starve media) for 2 hours. Cells were pelleted and resuspended in either BaF starve media with 10ug/mL heparin only (unstimulated or "-") or BaF starve media with heparin and 1nM rFGF2 (stimulated or "+") for 10 minutes at 37^{o}C. After 10 minutes, the cells were pelleted by brief centrifugation and immediately lysed in ice cold lysis buffer. Twenty micrograms total protein was resolved on a 4-12% Bis Tris gel and probed for

phosho p44/42 MAPK. Blots were then stripped and reprobed for total p44/42 MAPK (Cell Signaling Technologies).

Phosphorylation was quantitated using Image J (http://rsb.info.nih.gov/ij/) and presented as the ratio of phosporylated over total p44/42 MAPK for each mutant divided by the same ratio for the FGF2 stimulated wild type receptor.

Acknowledgements

We would like to thank Nick Hayward, Peter Parsons, Chris Schmidt and Kathy Brown for supplying melanoma cell lines, Dr Daniel Donoghue for providing FGFR2 expression constructs, and Michael Berens for helpful discussions and critical reading of the manuscript. This work was supported by funding from the Harry J Lloyd Charitable Trust, the Melanoma Research Foundation and the Leslie Ann Ballard Foundation (to P.P.). This work was also supported by NIH grant 2R01 DE 13686-08 (to M. M.) and an American Cancer Society Post Doctoral Fellowship PF-07-215-01-TBE grant (to S. B.).

Figure legends:

Figure. 1. Mapping of **FGFR2c extracellular mutations identified in melanoma tumors/cell lines onto the known FGF-FGFR crystal structures suggests that these mutations should impair FGFR2c activity.** The locations of mutated residues in the extracellular region of FGFR2 are mapped onto the ribbon diagram of 2:2:2 FGF2–FGFR1c–heparin complex (PDB ID: 1FQ9) (Schlessinger et al., 2000). FGF is colored orange and the extracellular ligand binding region of FGFR is colored as follows: D2 in green, D3 in cyan, D2–D3 linker in grey. The two heparin oligosaccharides in the dimer are rendered in sticks. To assist the viewer, certain β strands of D2 and D3 domains are labeled. Panels **A** through **E**, depict close-up view of the region where the mutated receptor residues are located. In each panel, in addition to the mutated residue, other relevant receptor residues are shown as ball-and-sticks. In panel **A**, the molecular interactions of G226 and V247, which correspond to the mutated G228 and V248 in FGFR2, are shown. G226 in βF strand makes hydrogen bonds with L245 in bG strand and contributes to proper βF-βG strand pair formation, and hence to overall stability of D2. V247 engages in hydrophobic contacts with other residues in the interior core of D2 and thus plays a critical role in folding of D2 as well. To emphasize these hydrophobic contacts, the surface of V247 and neighboring residues are shown in cyan (V247) and purple meshes, respectively. In panel **B**, R250, homologous to R251 in FGFR2, makes three hydrogen bonds with FGF ligand. Mutation of R251 to Q should substantially reduce binding affinity of mutated FGFR2 towards FGF ligand. In panel **C**, the molecular environments of G270 and N304 in FGFR1, which correspond to the mutated G271 and G305 in FGFR2, are shown. G270 plays a role in formation of turn between βA' and βB by making hydrogen bonds with other residues in D3. Therefore, mutation of G271 in FGFR2 should negatively impact the tertiary folding of D3. N304, on the other hand maps to the large loop region between strand βC and βC' which protrudes from D3 and does not play

any apparent role in structural integrity of D3. In panel **C**, the surfaces of the conserved cysteines (C277 and C341) in the interior core of D3 are shown as grey mesh. In panel D, the proximity of E159 and T212 to the heparin oligosaccharide chains in the dimer is emphasized. E159 and T212 correspond to E160 and H213 in FGFR2 respectively and mutation of these residues in melanoma could alter interaction of mutated FGFR2s with heparin/heparan sulfate. Panel **E** highlights the important role D2ι8 plays in binding of second FGF in the 2:2 FGF–FGFR dimer and hence dimerization. Mutation of E219 in FGFR2, which corresponds to D218 in FGFR1, should negatively impact the ability of receptor to undergo ligand- and HS-induced dimerization. Atom coloring is as follows: nitrogen in blue, oxygen in red, and sulfur in yellow. Hydrogen bonds are shown as dashed lines. Letters N and C denote the N- and C-termini of FGFR1c, respectively.

Figure. 2. FGFR2c kinase domain mutations identified in melanoma tumors/cell lines mapped onto the crystal structures of the FGFR2 kinase domain suggests that these mutations should impair the kinase activity of FGFR2. The positions of the mutated residues are mapped onto the crystal structure of unphosphorylated wild type FGFR2 kinase domain (PDB entry: 2PSQ) (15). The coloring of the intracellular tyrosine kinase domain is as follows: the N-terminal lobe of kinase in light blue, the C-terminal lobe in bright blue, the activation loop is in magenta, the kinase hinge region is in green and the N-terminal tail of the kinase is colored wheat. Note that ATP (not shown) binds in the cleft between the N-lobe and C-lobe of the kinase domain. To assist the viewer, certain β strands and α helices, that are relevant for explanation of the effects of the melanoma mutations, are labeled. Panel **A** shows that E636, which maps to the sharp turn between β7 and β8 strands, makes hydrogen bond with S563 in the kinase hinge region. Mutation of this residue to lysine could influence the relative disposition of N-lobe to C-lobe, and hence alter the tyrosine kinase activity of FGFR2. Panel **B** shows that the M640 and I642 side chains (red mesh) point into inner hydrophobic core of

kinase domain, and engage C606 and M614 (cyan mesh). Mutation of either M640 or I642 to smaller hydrophobic residues should weaken the extent of these core hydrophobic contacts and lead to reduction in kinase activity. In panel **C**, the hydrogen bonds between R759 and side chains of negatively charged E731 (in helix αH) and D756 (in helix αI) are shown. In addition to the loss of these hydrogen bonds, introduction of stop codon at this location will also truncate the helix αI by one helical turn. These structural changes should reduce the stability of kinase domain specifically making kinase domain temperature-sensitive, and ultimately lead to receptor loss-of-function. Panel **D** shows a close up view of the region where E475 is located. The side chain of E475 engages in two strong hydrogen bonds with side chain and backbone atom of T555 (located in the loop between β4 and β5 strand), which facilitate the conformation of the β4-β5 loop as well of the region preceding E475 itself. This in turn promotes the hydrophobic contacts between L468, T555 (the methyl group) and L560 from these regions and L528, V532 and M535 in the catalytically important αC helix. To emphasize this point, the side chains of these hydrophobic residues are shown as colored mesh. Panel **E** shows the close up view of the region where D530 and A648 are located. In unphosphorylated wild type FGFR2K structure, D530 does not play any role. However, in the A-loop phosphorylated activated FGFR2K structure (PDB entry: 2PVF)(15) the side chain of D530 engages in salt bridge with R664 in the A-loop and contributes to A-loop conformation in the 'Active' state (not shown). The side chain of A648, located at the beginning of A-loop, packs against the hydrophobic side chains of M537 in αC helix. Replacement of A648 with threonine is expected to lead to loss-of-function since the larger side chain of threonine will impede αC helix from nearing sufficiently close enough to the A-loop in the "Active" FGFR2K. Panel **F** shows close up view of the kinase region where G701 is located. G701 plays a role in stabilizing the conformation of the loop between the helices αF and αG, which is in hydrogen bonding contacts with K668 in the A-loop.

The G701S mutation should destabilize the αF-αG loop and indirectly affect the A-loop conformation.

Figure 3. SPR analysis shows that the R251Q mutation abrogates ligand binding. **(a-b)** Increasing concentrations of WT (**a**) or R251Q FGFR2c mutant ectodomain (b) were injected over a CM5 chip onto which full length human FGF2 was immobilized. The biosensor chip response is plotted as a function of time. SPR analysis performed as previously described (18).

Figure 4. FGFR2 kinase domains harboring melanoma mutations have reduced tyrosine autophosphorylation activity. Wild-type FGFR2K and four mutant FGFR2Ks each harboring E475K, D530N, I642V, or A648T single mutation, are subjected to *in vitro* kinase assays. Data represent the average of three independent experiments plus standard deviations. The tyrosine autophosphorylation activity of these wild-type and mutant FGFR2Ks were determined using a continuous spectrophotometric assay as previously described (42).

Figure 5. **Mutations in FGFR2 impair receptor processing and localization (a)** Confirmation of post translational glycosylation of wild type FGFR2 by PNGase digestion of both the 130kDa band (solid arrow)and 110 kDa band (stippled arrow) to a single 98 kDa band (open arrow) in HEK293 cells. Sensitivity to digestion with $EndoH_f$ of only the 110 kDa band indicates this 110 kDa band to be immature, partially processed receptor predominantly present in the ER and early Golgi. **(b)** $EndoH_f$ digestion of FGFR2 in HEK293 lysates transiently transfected with wildtype FGFR2 or mutant FGFR2. Densitometry analysis revealed that the EndoH resistant 130 kDa band comprises ~60% of the wildtype FGFR2 but only 30% of G227E, V248D, G271E, and C278F mutants. **(c)** Localization of wildtype and mutated FGFR2 following transient transfection into HEK293 cells and immunofluorescent staining. Impaired receptor trafficking is evident for

G227E, V248D, G271E and C278F compared to trafficking of the wildtype receptor to the cell surface. **(d)** Immunofluorescent analysis of the colocalization of FGFR2 (red, left panels) and the ER resident marker PDI (green, middle panels) confirms the overall retention of the G227E mutant receptor in the ER compartment in HEK293 cells (yellow, right panel) when compared with the cell surface localization of wildtype FGFR2 and E219K (mapping onto the known extracellular crystal structure predicted the latter mutation to have no effect on misfolding).

Figure 6. Cell proliferation in response to FGF2 in BaF3 cell lines stably transduced with wildtype and mutant FGFR2_IRES_Neo expression constructs.

(a) All novel mutations identified in melanoma result in a decrease in BaF3 proliferation when compared to wild type FGFR2. Gray bars indicate basal proliferation in the absence of ligand and black bars represent proliferation in response to 1nM FGF2. Data represents the average of at least two independent experiments assayed in triplicate. (b) Analysis of phospho p44/42 MAPK upon stimulation with exogenous rFGF-2 shows that with the exception of the N549K positive control, mutations impair the ability of the receptor to activate this pro-proliferation pathway compared to wild type receptor. (c) Western blot showing equal expression of FGFR2 by all mutants except empty vector in the absence (-) and presence (+) of FGF2. (d) Graphical representation of p44/42 MAPK phosphorylation expressed as a percentage of phosphorylation (upon ligand stimulation) of that of wild type receptor.

Figure 7. Reintroduction of FGFR2 failed to suppress proliferation of $SbCl_2$ or AO4 melanoma cells.

(a) Melanoma cell lines SbCl2 and AO4 were stably transduced with empty vector, FGFR2, or FGFR2 K517R lentivirus and proliferation was assessed using the sulforhodamine B (SRB) assay. Overexpression of FGFR2 or kinase dead FGFR2 K517R had no effect on the

proliferation of these melanoma cell lines. **(b)** FGFR2 expression was confirmed by Western blot analysis.

Figure 8. Schematic representation of FGFR2 mutations highlighting the difference spectrum of somatic mutations in melanoma compared to endometrial cancer and also germline mutations in craniosynostosis syndromes.

(a) Novel somatic mutations in FGFR2 identified in melanoma cell lines and uncultured tumors are presented in red above the schematic representation of the protein and numbered relative to FGFR2c (NP_000132.1). **(b)** Somatic mutations in FGFR2 identified in primary endometrial cancers and cell lines are presented in green (upper panel) above the schematic representation of the protein and are numbered relative to FGFR2b (NP_075259.2) (12). Germline mutations associated with a variety of craniosynostosis syndromes and numbered relative to FGFR2c (NP_000132.1) are presented in the lower panel (http://www.hgmd.cf.ac.uk/ac/index.php). Novel mutations are underlined. Four somatic FGFR2 endometrial mutations, while not previously reported in the germline, have an identical missense change reported in the paralogous position in FGFR3c in a skeletal chondrodysplasia (indicated with **) (http://www.hgmd.cf.ac.uk/ac/index.php). Note that the majority of somatic mutations in endometrial cancer parallel those identified in the germline while every melanoma mutation was novel.

Table 1. Summary of melanoma samples carrying FGFR2 mutations

Samples	Nucleotide change	Codon change	BRAF	NRAS
Cell Lines				
MM540	G812A	G271E	V600E	wt
UACC1940	G913A	G305R	wt	wt
WSB	C1109G	T370R[b]	V600E	wt
M92-001 [a]	G1423A	E475K[b]	wt	G13R
ME10538[a]	G1423A	E475K	V600E	wt
M91-054	T2308G	L770V	V600E	wt
UACC2534	G752A	R251Q	wt	wt
A375	G1906A	E636K[b]	V600E	wt
UACC3093	GG2100-1AA	G701S	wt	Q61L
D11	G1920A	M640I	wt	Q61L
MM369	G655A	E219K	V600E	wt
D22	G1588A	D530N	wt	wt
D22	C2275T	R759X	wt	wt
MM229	G2276A	R759Q	L597S	wt
A04	G1942A	A648T[b]	wt	wt
A05	A479C	E160A	V600E	wt
Metastatic Tumors				
Met19	G680A	G227E	wt	nd
Met27	C71T	S24F	nd	nd
Met15	G229A G1720A C2063T C2122T	V77M E574K S688F P708S	V600E	nd
Primary Tumors				
81[c]	IVS15-2A>T [g]	FS	V600E	wt
AM169 [d]	T743A	V248D	wt	wt
AM146 [e]	C637T	H213Y	wt	Q61L
53 [f]	G1422A	W474X	wt	wt
71 [f]	G1924A	I642V	wt	wt

[a]Microsatellite genotyping confirmed these cell lines were independent; [b]samples were homozygous for this mutation. [c] SSM primary melanoma, no chronic sun damage evident; [d] Acral melanoma, histologically SSM; [e] Mucosal primary melanoma; [f] Primary Lentigo Maligna Melanoma, with histological evidence of chronic sun damage. Nd, not done. [g] The IVS15-2A>T is predicted to result in the skipping of exon 16, subsequent frameshift for 27aa and a premature truncation at codon 690 in the kinase domain.

Table 2. Summary of in-silico analysis of FGFR2 mutations

Novel FGFR2 mutation	Predicted effect based on molecular modeling
E160A, H213Y	Negatively impact interaction with HS
E219K	Reduced FGF and heparin mediated receptor dimerization
G227E, V248D	Destabilize the D2 domain
R251Q	Abrogate ligand binding
G271E	Destabilize the D3 domain
E475K	Possible increased kinase activity but less stable kinase domain
M640I, I642V	Local structural perturbations resulting in altered conformation of the activation loop and decreased kinase activity
A648T	Markedly reduced kinase activity due to misalignment of catalytic residues for phosphotransfer reaction
L770V	Impaired phosphorylation of Y769 and reduced recruitment of PLCγ

REFERENCES

1. Halaban R. Growth factors and melanomas. Semin Oncol 1996;23(6):673-81.
2. Lazar-Molnar E, Hegyesi H, Toth S, Falus A. Autocrine and paracrine regulation by cytokines and growth factors in melanoma. Cytokine 2000;12(6):547-54.
3. Ornitz DM, Itoh N. Fibroblast growth factors. Genome Biol 2001;2(3):REVIEWS3005.
4. Nesbit M, Nesbit HK, Bennett J, *et al.* Basic fibroblast growth factor induces a transformed phenotype in normal human melanocytes. Oncogene 1999;18(47):6469-76.
5. Meier F, Caroli U, Satyamoorthy K, *et al.* Fibroblast growth factor-2 but not Mel-CAM and/or beta3 integrin promotes progression of melanocytes to melanoma. Exp Dermatol 2003;12(3):296-306.
6. Halaban R, Kwon BS, Ghosh S, Delli Bovi P, Baird A. bFGF as an autocrine growth factor for human melanomas. Oncogene Res 1988;3(2):177-86.
7. Becker D, Meier CB, Herlyn M. Proliferation of human malignant melanomas is inhibited by antisense oligodeoxynucleotides targeted against basic fibroblast growth factor. EMBO J 1989;8(12):3685-91.
8. Becker D, Lee PL, Rodeck U, Herlyn M. Inhibition of the fibroblast growth factor receptor 1 (FGFR-1) gene in human melanocytes and malignant melanomas leads to inhibition of proliferation and signs indicative of differentiation. Oncogene 1992;7(11):2303-13.
9. Xerri L, Battyani Z, Grob JJ, *et al.* Expression of FGF1 and FGFR1 in human melanoma tissues. Melanoma Res 1996;6(3):223-30.
10. Wang Y, Becker D. Antisense targeting of basic fibroblast growth factor and fibroblast growth factor receptor-1 in human melanomas blocks intratumoral angiogenesis and tumor growth. Nat Med 1997;3(8):887-93.
11. Valesky M, Spang AJ, Fisher GW, Farkas DL, Becker D. Noninvasive dynamic fluorescence imaging of human melanomas reveals that targeted inhibition of bFGF or FGFR-1 in melanoma cells blocks tumor growth by apoptosis. Mol Med 2002;8(2):103-12.
12. Pollock PM, Gartside MG, Dejeza LC, *et al.* Frequent activating FGFR2 mutations in endometrial carcinomas parallel germline mutations associated with craniosynostosis and skeletal dysplasia syndromes. Oncogene 2007;26(50):7158-62.
13. Stephens P, Edkins S, Davies H, *et al.* A screen of the complete protein kinase gene family identifies diverse patterns of somatic mutations in human breast cancer. Nat Genet 2005;37(6):590-2.
14. Schlessinger J, Plotnikov AN, Ibrahimi OA, *et al.* Crystal structure of a ternary FGF-FGFR-heparin complex reveals a dual role for heparin in FGFR binding and dimerization. Mol Cell 2000;6(3):743-50.
15. Chen H, Ma J, Li W, *et al.* A molecular brake in the kinase hinge region regulates the activity of receptor tyrosine kinases. Mol Cell 2007;27(5):717-30.
16. Ibrahimi OA, Eliseenkova AV, Plotnikov AN, Yu K, Ornitz DM, Mohammadi M. Structural basis for fibroblast growth factor receptor 2 activation in Apert syndrome. Proc Natl Acad Sci U S A 2001;98(13):7182-7.
17. Yu K, Herr AB, Waksman G, Ornitz DM. Loss of fibroblast growth factor receptor 2 ligand-binding specificity in Apert syndrome. Proc Natl Acad Sci U S A 2000;97(26):14536-41.
18. Ibrahimi OA, Zhang F, Eliseenkova AV, Itoh N, Linhardt RJ, Mohammadi M. Biochemical analysis of pathogenic ligand-dependent FGFR2 mutations suggests distinct pathophysiological mechanisms for craniofacial and limb abnormalities. Hum Mol Genet 2004;13(19):2313-24.

19. Hatch NE, Hudson M, Seto ML, Cunningham ML, Bothwell M. Intracellular retention, degradation, and signaling of glycosylation-deficient FGFR2 and craniosynostosis syndrome-associated FGFR2C278F. J Biol Chem 2006;281(37):27292-305.
20. Meyer AN, Gastwirt RF, Schlaepfer DD, Donoghue DJ. The cytoplasmic tyrosine kinase Pyk2 as a novel effector of fibroblast growth factor receptor 3 activation. J Biol Chem 2004;279(27):28450-7.
21. Naski MC, Wang Q, Xu J, Ornitz DM. Graded activation of fibroblast growth factor receptor 3 by mutations causing achondroplasia and thanatophoric dysplasia. Nat Genet 1996;13(2):233-7.
22. Julies MG, Moore SW, Kotze MJ, du Plessis L. Novel RET mutations in Hirschsprung's disease patients from the diverse South African population. Eur J Hum Genet 2001;9(6):419-23.
23. Rohmann E, Brunner HG, Kayserili H, *et al.* Mutations in different components of FGF signaling in LADD syndrome. Nat Genet 2006;38(4):414-7.
24. Shams I, Rohmann E, Eswarakumar VP, *et al.* Lacrimo-auriculo-dento-digital syndrome is caused by reduced activity of the fibroblast growth factor 10 (FGF10)-FGF receptor 2 signaling pathway. Mol Cell Biol 2007;27(19):6903-12.
25. Lew ED, Bae JH, Rohmann E, Wollnik B, Schlessinger J. Structural basis for reduced FGFR2 activity in LADD syndrome: Implications for FGFR autoinhibition and activation. Proc Natl Acad Sci U S A 2007;104(50):19802-7.
26. L'Hote CG, Knowles MA. Cell responses to FGFR3 signalling: growth, differentiation and apoptosis. Exp Cell Res 2005;304(2):417-31.
27. Logie A, Dunois-Larde C, Rosty C, *et al.* Activating mutations of the tyrosine kinase receptor FGFR3 are associated with benign skin tumors in mice and humans. Hum Mol Genet 2005;14(9):1153-60.
28. Grose R, Fantl V, Werner S, *et al.* The role of fibroblast growth factor receptor 2b in skin homeostasis and cancer development. EMBO J 2007;26(5):1268-78.
29. Yamaguchi F, Saya H, Bruner JM, Morrison RS. Differential expression of two fibroblast growth factor-receptor genes is associated with malignant progression in human astrocytomas. Proc Natl Acad Sci U S A 1994;91(2):484-8.
30. Naimi B, Latil A, Fournier G, Mangin P, Cussenot O, Berthon P. Down-regulation of (IIIb) and (IIIc) isoforms of fibroblast growth factor receptor 2 (FGFR2) is associated with malignant progression in human prostate. Prostate 2002;52(3):245-52.
31. Diez de Medina SG, Chopin D, El Marjou A, *et al.* Decreased expression of keratinocyte growth factor receptor in a subset of human transitional cell bladder carcinomas. Oncogene 1997;14(3):323-30.
32. Ricol D, Cappellen D, El Marjou A, *et al.* Tumour suppressive properties of fibroblast growth factor receptor 2-IIIb in human bladder cancer. Oncogene 1999;18(51):7234-43.
33. Feng S, Wang F, Matsubara A, Kan M, McKeehan WL. Fibroblast growth factor receptor 2 limits and receptor 1 accelerates tumorigenicity of prostate epithelial cells. Cancer Res 1997;57(23):5369-78.
34. Matsubara A, Kan M, Feng S, McKeehan WL. Inhibition of growth of malignant rat prostate tumor cells by restoration of fibroblast growth factor receptor 2. Cancer Res 1998;58(7):1509-14.
35. Yasumoto H, Matsubara A, Mutaguchi K, Usui T, McKeehan WL. Restoration of fibroblast growth factor receptor2 suppresses growth and tumorigenicity of malignant human prostate carcinoma PC-3 cells. Prostate 2004;61(3):236-42.
36. Zhang Y, Wang H, Toratani S, *et al.* Growth inhibition by keratinocyte growth factor receptor of human salivary adenocarcinoma cells through induction of differentiation and apoptosis. Proc Natl Acad Sci U S A 2001;98(20):11336-40.
37. Fang X, Stachowiak EK, Dunham-Ems SM, Klejbor I, Stachowiak MK. Control of CREB-binding protein signaling by nuclear fibroblast growth factor receptor-1: a novel mechanism of gene regulation. J Biol Chem 2005;280(31):28451-62.

38. Kim Y, Bingham N, Sekido R, Parker KL, Lovell-Badge R, Capel B. Fibroblast growth factor receptor 2 regulates proliferation and Sertoli differentiation during male sex determination. Proc Natl Acad Sci U S A 2007;104(42):16558-63.
39. Ueno H, Gunn M, Dell K, Tseng A, Jr., Williams L. A truncated form of fibroblast growth factor receptor 1 inhibits signal transduction by multiple types of fibroblast growth factor receptor. J Biol Chem 1992;267(3):1470-6.
40. Kiselyov VV, Skladchikova G, Hinsby AM, *et al.* Structural basis for a direct interaction between FGFR1 and NCAM and evidence for a regulatory role of ATP. Structure 2003;11(6):691-701.
41. Rowland BD, Peeper DS. KLF4, p21 and context-dependent opposing forces in cancer. Nat Rev Cancer 2006;6(1):11-23.
42. Barker SC, Kassel DB, Weigl D, Huang X, Luther MA, Knight WB. Characterization of pp60c-src tyrosine kinase activities using a continuous assay: autoactivation of the enzyme is an intermolecular autophosphorylation process. Biochemistry 1995;34(45):14843-51.

Gartside et al. Figure 1.

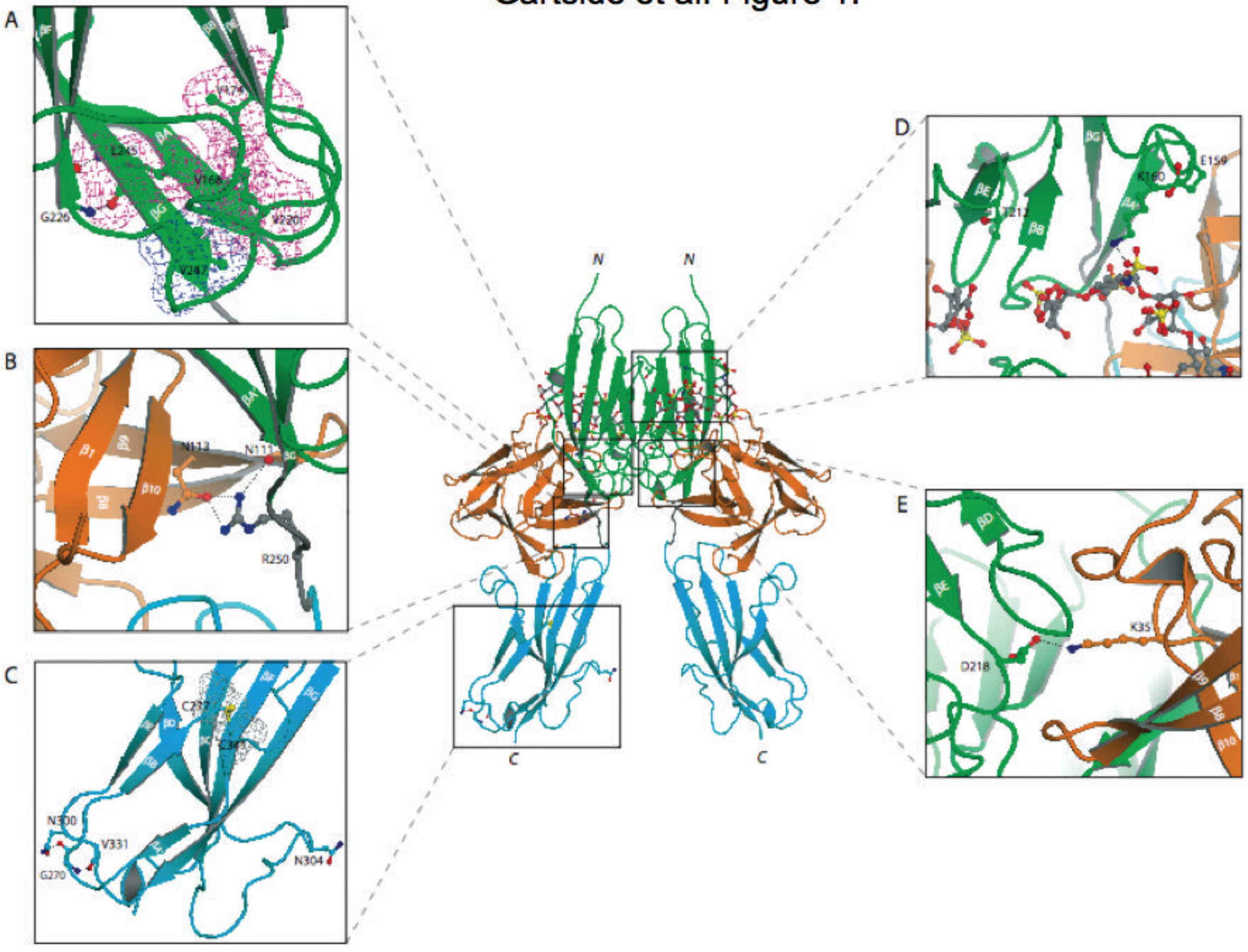

Gartside et al. Figure 2.

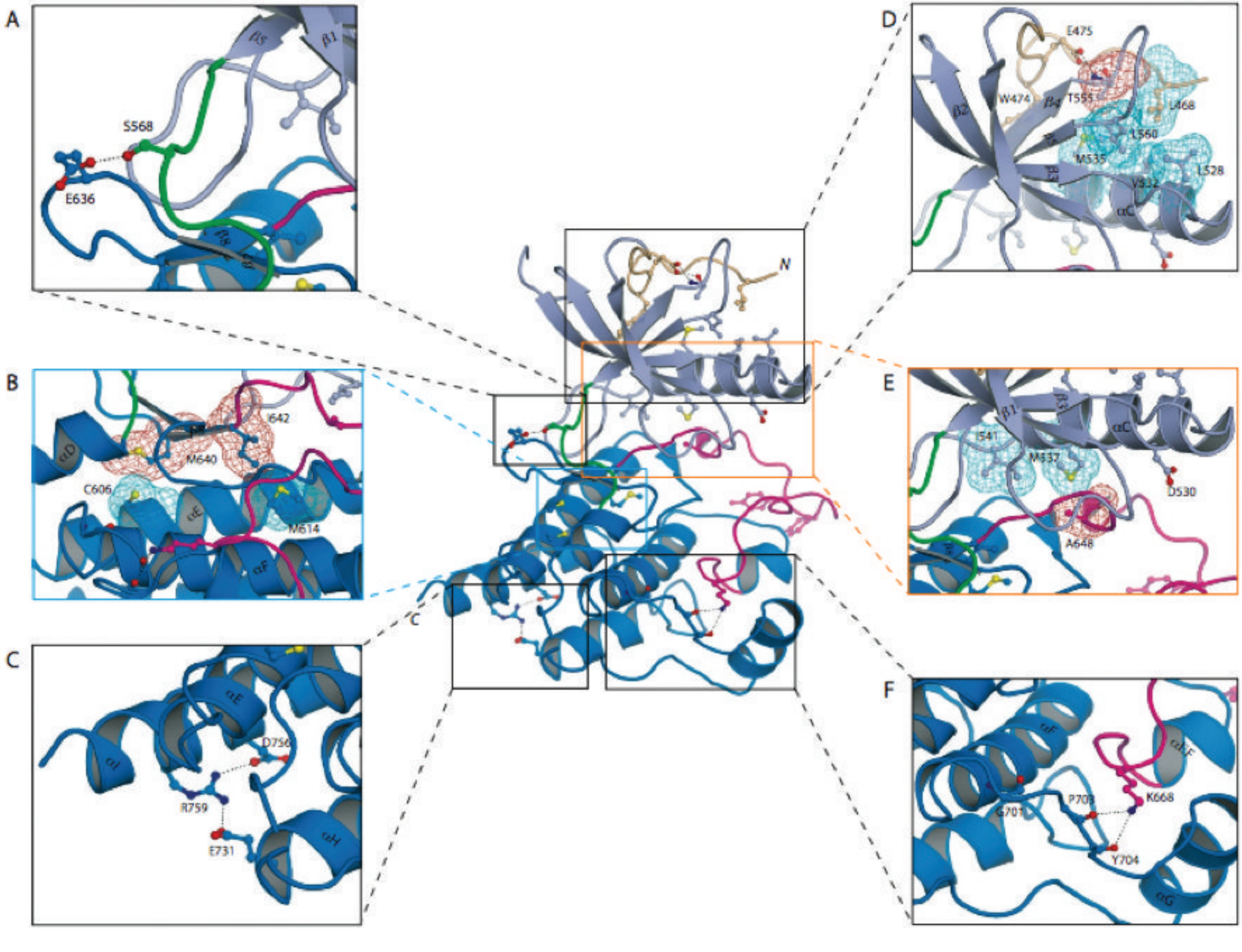

Gartside et al. Figure 3

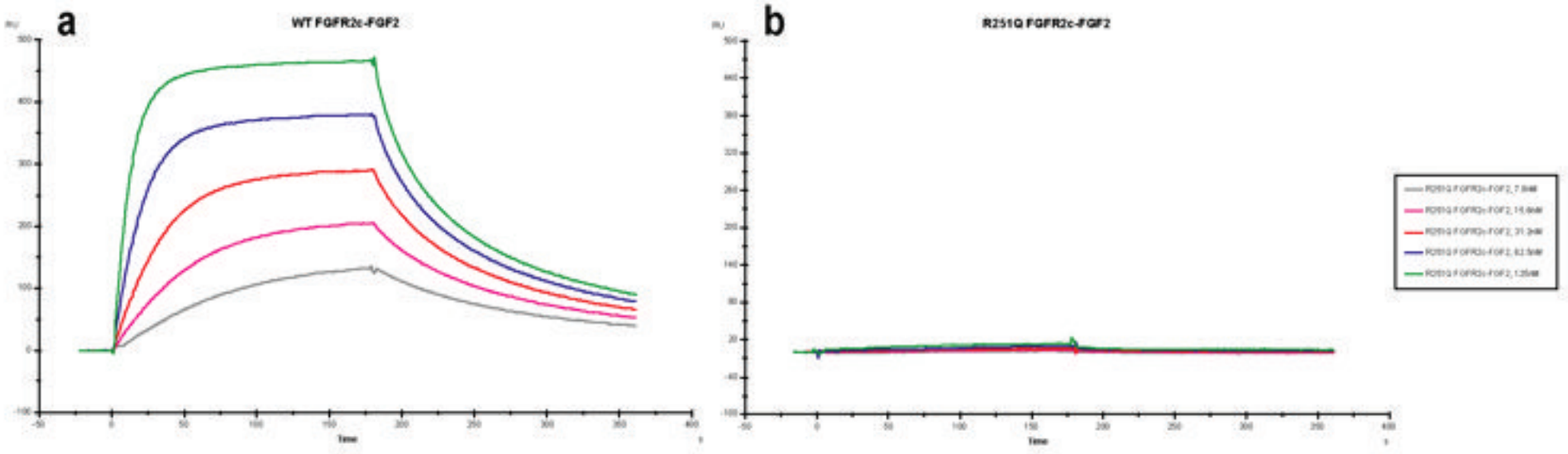

Gartside et al. Figure 4

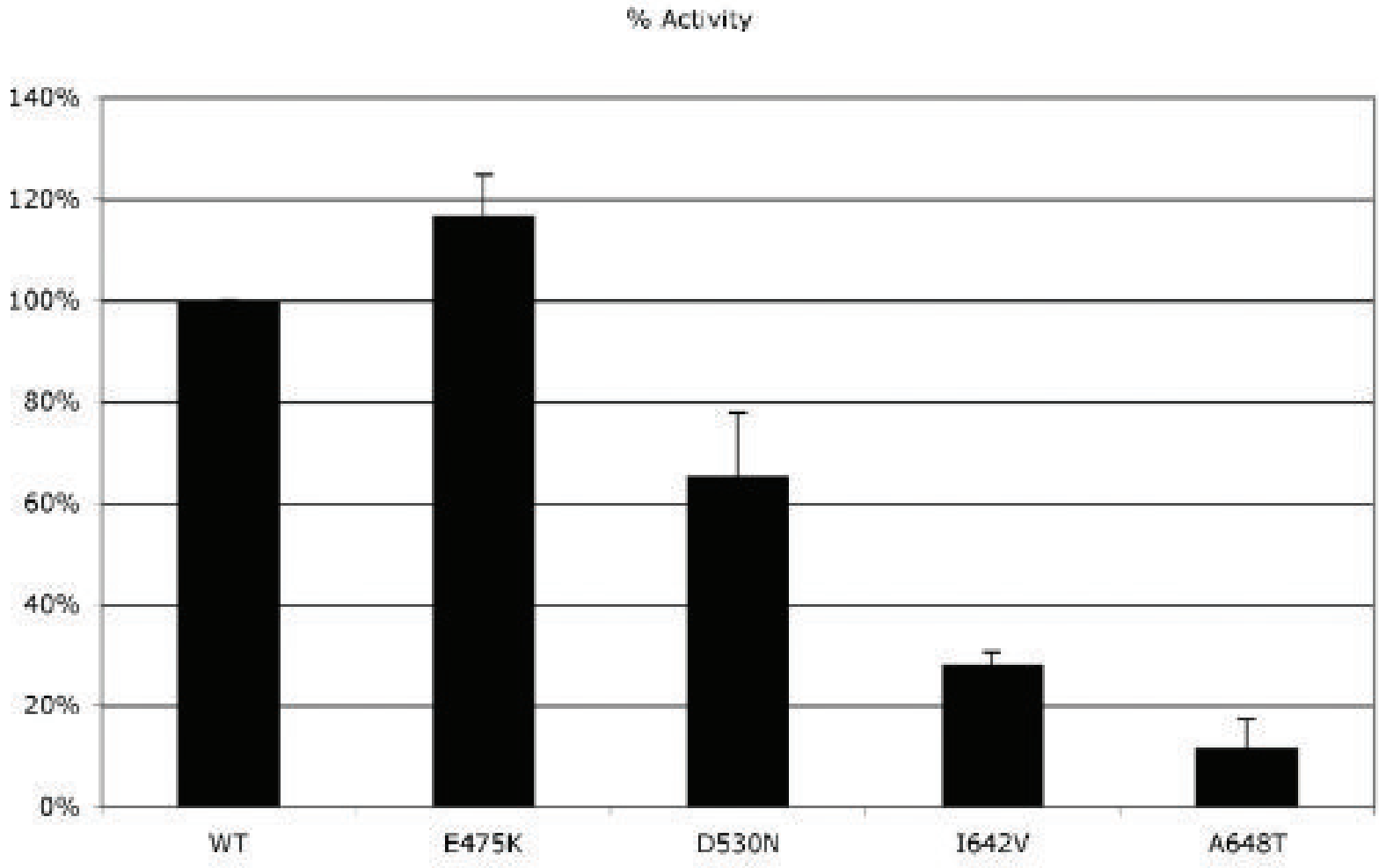

Gartside et al. Figure 5.

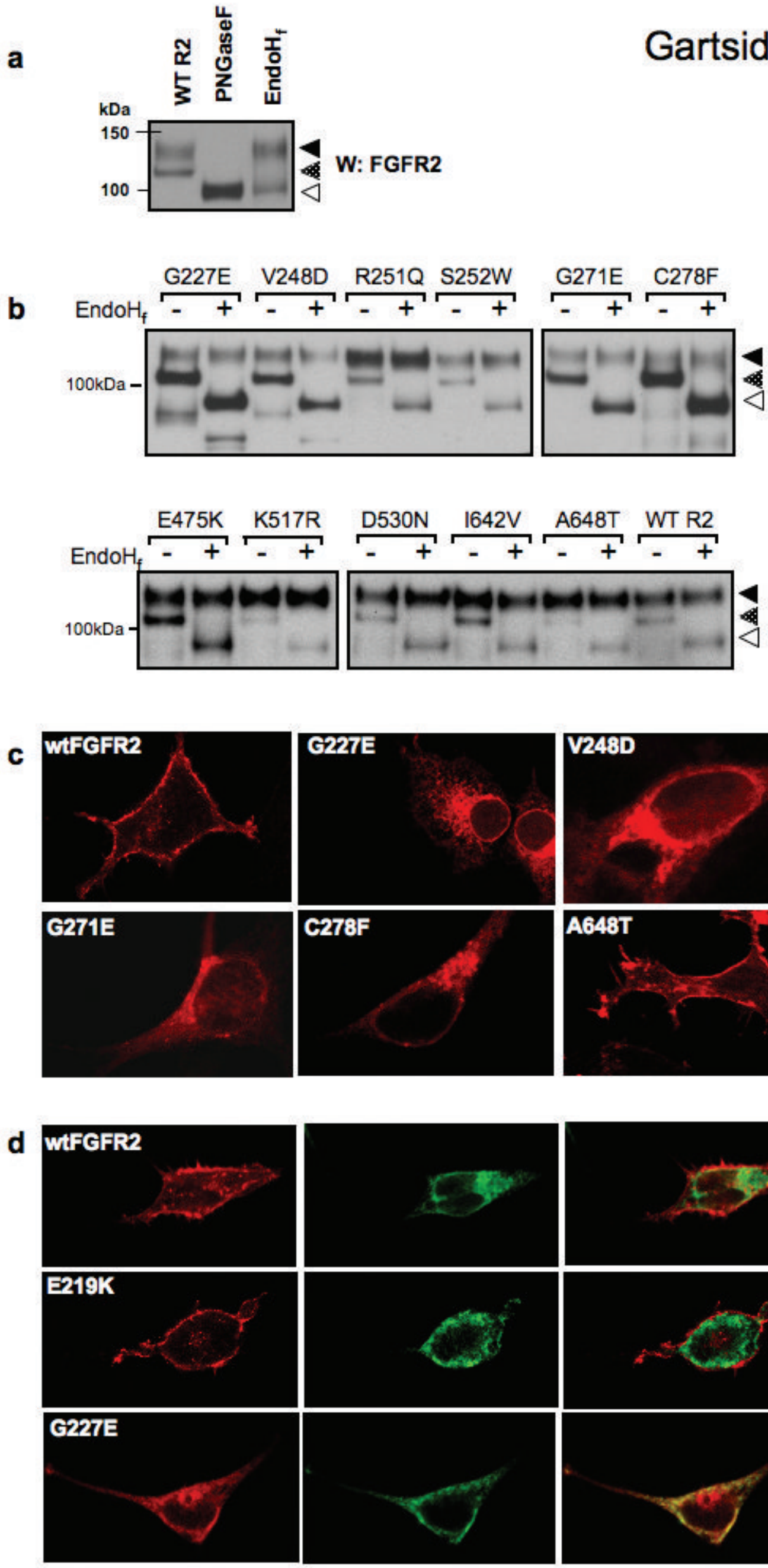

Gartside et al. Figure 6

a

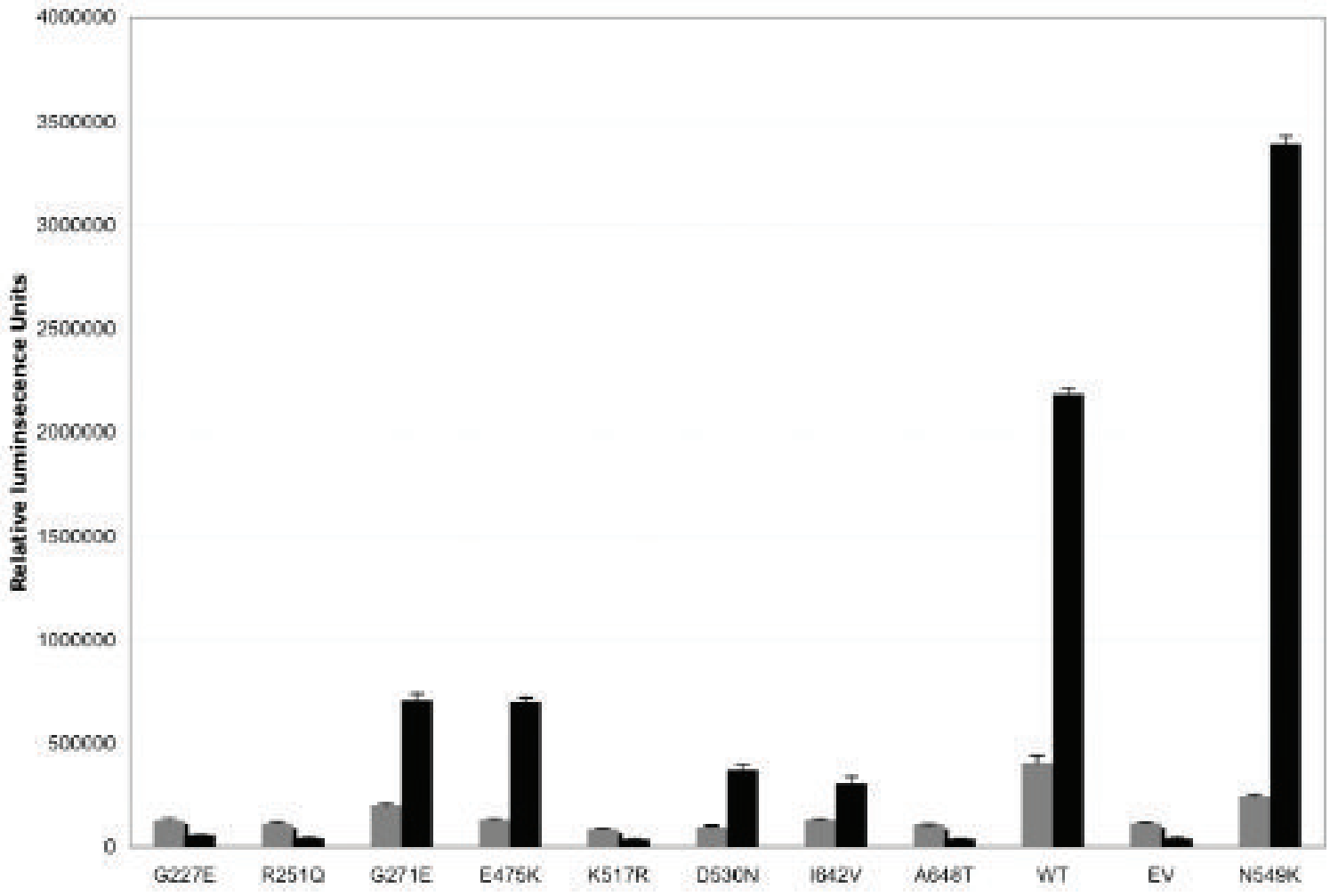

Gartside et al. Figure 6

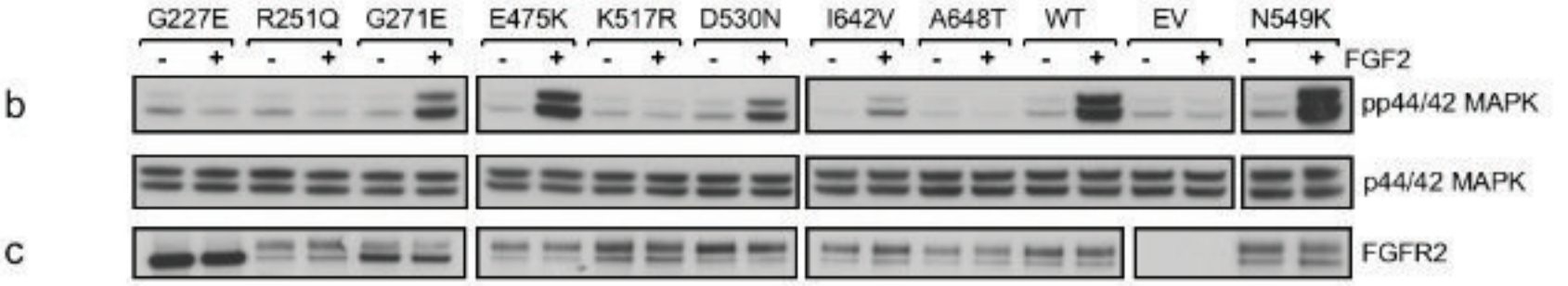

d

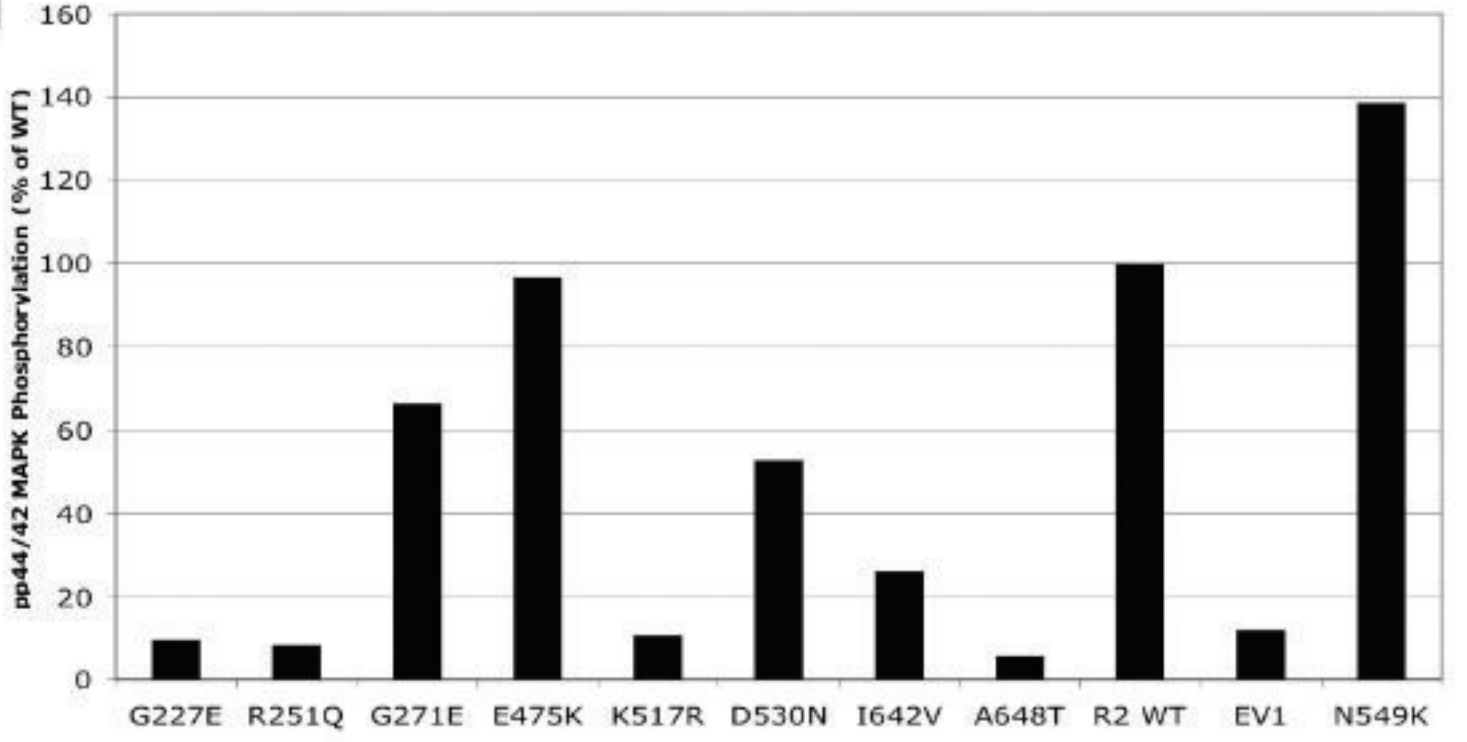

Gartside et al Figure 7 a & b

a

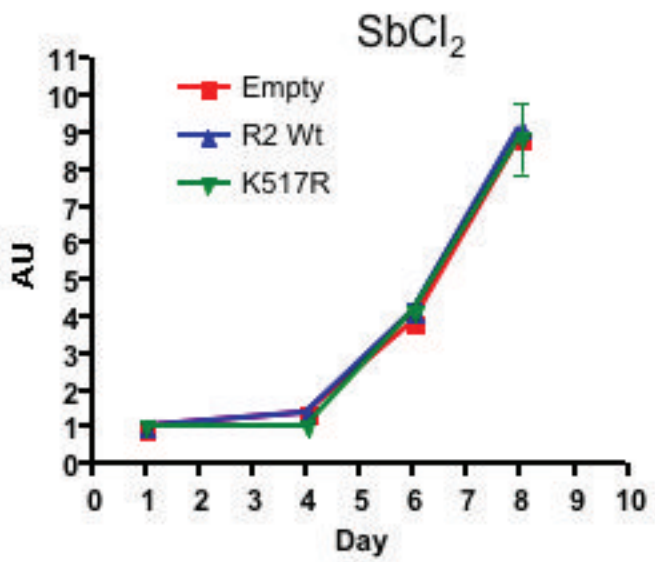

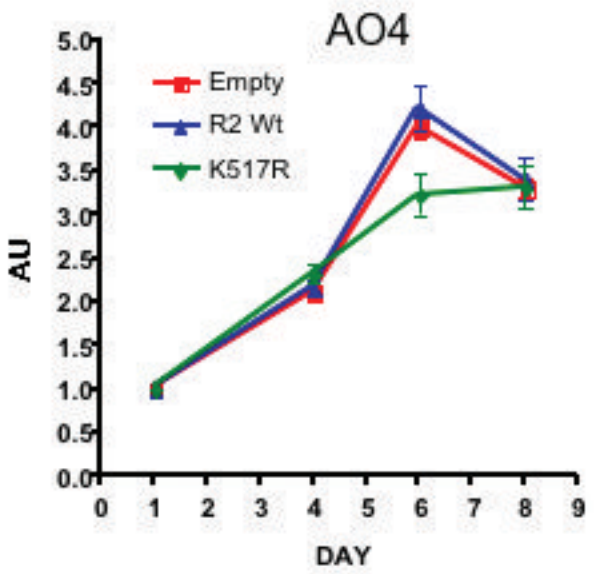

b

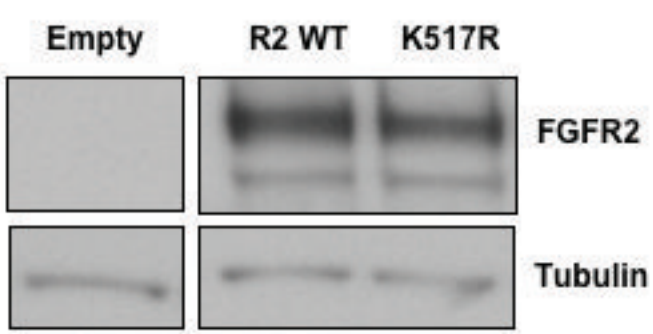

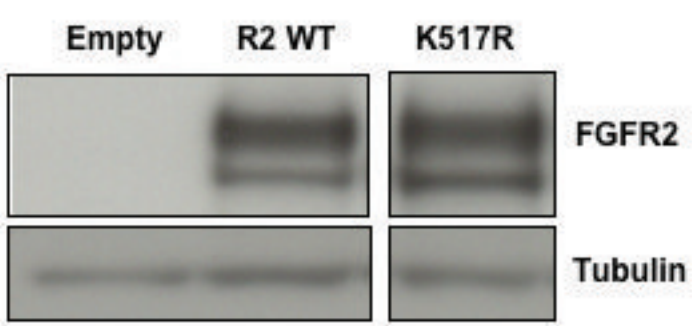

Gartside et al. Figure 8

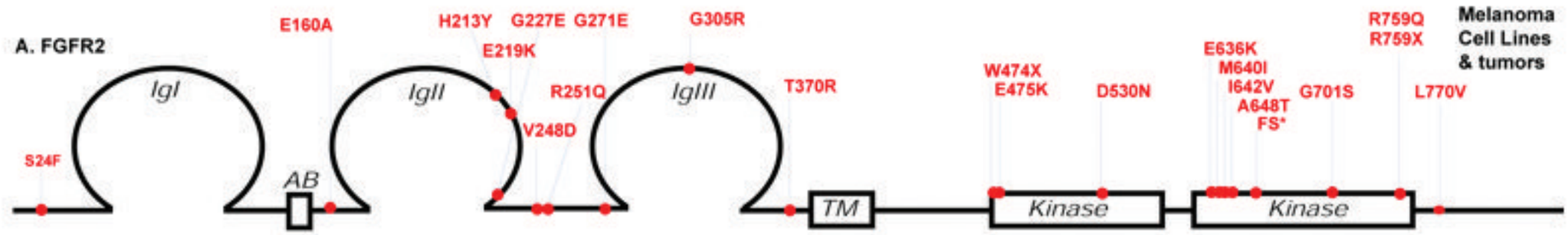

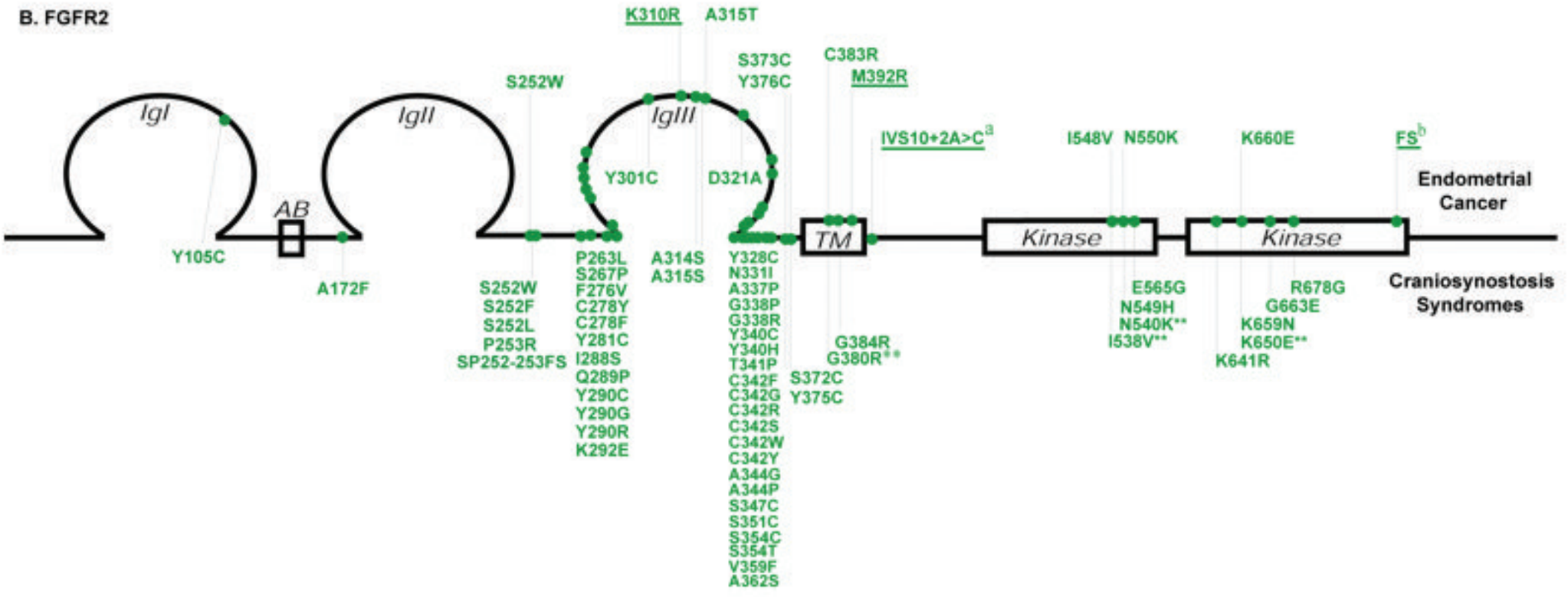

Supplemental Methods- Mutation Analysis

PCR .

The initial mutation screen included the majority of exons in FGFR1 and FGFR2. As virtually no mutations had even been reported in the N-terminal regions of the FGFRs, exons 1 and 2 were not screened for FGFR3 and exons 1-6 were not screened for FGFR4 (Summarized in Supplemental Table 2). Notably all exons in which the majority of activating mutations had previously been identified in the germline of FGFR1-3 were screened across all four genes. PCR primers were M13 tailed and sequences are available on request. New PCR primers were designed for FGFR2 for amplification from FFPE tissue.

Supplemental Table 2.

Gene Name	Reference Seqence	Exons Screened
FGFR1	NM_023110	Exons 2-18 (ATG in exon 2)
FGFR2	NM_00141	Exons 2-18 (ATG in exon 2)
FGFR2	NM_022970	Exon 8 (epithelially spliced exon)
FGFR3	NM_000142	Exons 3-17 (ATG in exon 1)
FGFR4	NM_213647	Exons 7-18 (ATG in exon 1)

dHPLC. 40 additional cell lines were screened for mutations in exons 6-18 of FGFR2 by DHPLC using the Transgenomic WAVE Nucleic Acid Fragment Analysis System. The base-pair sequence for each FGFR2 exon was imported in to the WAVEMAKER software to identify suitable denaturing conditions (conditions available on request). Prior to the samples being loaded, each sample was spiked 50:50 with a CEPH control to ensure the detection of both heterozygous and homozygous variants. At the completion of DHPLC, chromatograms were printed out and individually analyzed for the presence of a

potential variation. In those cases where identical DHPLC peak profiles were present in many samples, several cases were chosen for sequencing and in all cases a common SNP was present and not a mutation. PCR exons were either cleaned up using a PCR purification kit (Qiagen) and the BIOROBOT 9600 dual vacuum system (Qiagen) or purified after thermocycling using solid phase reversible immobilization (SPRI)-based technology (AMPure®; Agencourt Biosciences Corp., Beverly, MA), resulting in the removal of unincorporated dNTPs, primers, and salts. PCR products were eluted in 30µl distilled H_2O

Sequencing: Both strands of each PCR product were sequenced as follows: Sequencing reactions were performed using 3µl (approximately 25ng) of purified PCR product in a 6µl reaction containing 0.33µl BigDye Terminator v3.1 premix, 3.2 pmol of either M13 forward (TGTAAAACGACGGCCAGT) or M13 reverse (CAGGAAACAGCTATGACC) primer, and 1.03µl 5X BigDye sequencing buffer. Cycle-sequencing was performed for 35 cycles following the manufacturers recommendations on GeneAmp 9700 PCR machines (Applied Biosystems, Foster City, CA). Sequencing reactions were purified using CleanSEQ® (Agencourt Biosciences Corp., Beverly, MA) to remove unincorporated dye-terminators, and analyzed on 3730xl DNA analyzers (Applied Biosystems, Foster City, CA).

Sequence Analysis and Confirmation. We aligned and analyzed sequence chromatograms using Sequencher Version 4.1 (Gene Codes). All mutations were verified in an independent PCR amplification. For the primary tumors, DNA was extracted as

previously described [39]. Due to cccasional PCR failure and limiting DNA quantity, we were unable to sequence all 18 exons of FGFR2 for every tumor sample. Overall, about 85% of the coding region of FGFR2 was sequenced in the panel of primary tumors. PCR dropouts were repeated once and samples were included if they had less than 5 exons dropout. For three of these tumors, there was sufficient normal tissue from which to extract DNA and in all cases the mutation was only present in the tumor, confirming the somatic origin of these changes.

Supplementary Table 1 The following primers were used to introduce mutations

(sense, 5’ to 3’ with mutagenic changes underlined and silent substitutions in lower case):

E219K	CACTGGAGCCTCATTATG<u>A</u>AAAGTGTGGTaCCATCTGA
G227E	GGTCCCATCTGACAAGG<u>A</u>AAAcTATACaTGTGTGGTGGAG
V248D	ACACGTACCACCTGGATG<u>AC</u>GTcGAGCGATCGCCTCAC
R251Q	CTGGAcGTTGTcGAGC<u>A</u>ATCGCCTCACCGG
S252W	GTTGTGGAGCGcT<u>G</u>GCCTCACCGGC
G271E	CCTCCACAGTcGTCG<u>A</u>AGGAGACGTcGAGTTTG
C278F	TGGTCGGAGGAGACGTcGAGTTTGTCT<u>T</u>CAAGGTTTACAG
E475K	CCAGAGGAtCCAAAATGG<u>A</u>AGTTTCCAAGAGATAAGCTG
D530N	ACAGAGAAAGACCTTTCT<u>A</u>ATCTGGTcTCAGAGATGG
I642V	CAGAAAACAATGTcATGAAA<u>G</u>TAGCAGACTTTGGACTCG
A648T	TAGCAGACTTTGGtCTC<u>A</u>CCAGAGATATCAACAATATAGAC
N549K	CACAAGAATATCATAAA<u>g</u>CTTCTTGGAGCCTGCACAC